NASA/TP-2000-210085
AFDD/TR-00-A-004

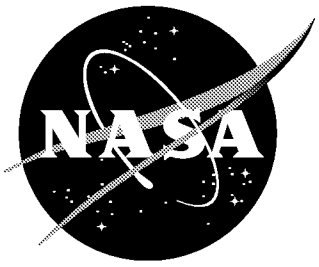

Flow Environment Study Near the Empennage of a 15-Percent Scale Helicopter Model

Susan Althoff Gorton
Langley Research Center
Hampton, Virginia

John D. Berry
Directorate of Aviation Engineering
US Army Aviation and Missile Command
Redstone Arsenal, Huntsville, Alabama

W. Todd Hodges and Deane G. Reis
Aeroflightdynamics Directorate
US Army Aviation and Missile Command
Langley Research Center, Hampton, Virginia

March 2000

The NASA STI Program Office ... in Profile

Since its founding, NASA has been dedicated to the advancement of aeronautics and space science. The NASA Scientific and Technical Information (STI) Program Office plays a key part in helping NASA maintain this important role.

The NASA STI Program Office is operated by Langley Research Center, the lead center for NASA's scientific and technical information. The NASA STI Program Office provides access to the NASA STI Database, the largest collection of aeronautical and space science STI in the world. The Program Office is also NASA's institutional mechanism for disseminating the results of its research and development activities. These results are published by NASA in the NASA STI Report Series, which includes the following report types:

- TECHNICAL PUBLICATION. Reports of completed research or a major significant phase of research that present the results of NASA programs and include extensive data or theoretical analysis. Includes compilations of significant scientific and technical data and information deemed to be of continuing reference value. NASA counterpart of peer-reviewed formal professional papers, but having less stringent limitations on manuscript length and extent of graphic presentations.

- TECHNICAL MEMORANDUM. Scientific and technical findings that are preliminary or of specialized interest, e.g., quick release reports, working papers, and bibliographies that contain minimal annotation. Does not contain extensive analysis.

- CONTRACTOR REPORT. Scientific and technical findings by NASA-sponsored contractors and grantees.

- CONFERENCE PUBLICATION. Collected papers from scientific and technical conferences, symposia, seminars, or other meetings sponsored or co-sponsored by NASA.

- SPECIAL PUBLICATION. Scientific, technical, or historical information from NASA programs, projects, and missions, often concerned with subjects having substantial public interest.

- TECHNICAL TRANSLATION. English-language translations of foreign scientific and technical material pertinent to NASA's mission.

Specialized services that complement the STI Program Office's diverse offerings include creating custom thesauri, building customized databases, organizing and publishing research results ... even providing videos.

For more information about the NASA STI Program Office, see the following:

- Access the NASA STI Program Home Page at ***http://www.sti.nasa.gov***

- E-mail your question via the Internet to help@sti.nasa.gov

- Fax your question to the NASA STI Help Desk at (301) 621-0134

- Phone the NASA STI Help Desk at (301) 621-0390

- Write to:
  NASA STI Help Desk
  NASA Center for AeroSpace Information
  7121 Standard Drive
  Hanover, MD 21076-1320

NASA/TP-2000-210085
AFDD/TR-00-A-004

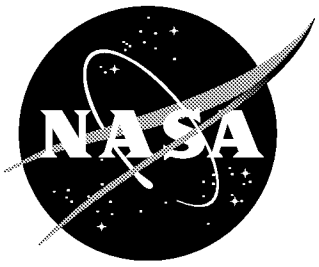

Flow Environment Study Near the Empennage of a 15-Percent Scale Helicopter Model

Susan Althoff Gorton
Langley Research Center
Hampton, Virginia

John D. Berry
Directorate of Aviation Engineering
US Army Aviation and Missile Command
Redstone Arsenal, Huntsville, Alabama

W. Todd Hodges and Deane G. Reis
Aeroflightdynamics Directorate
US Army Aviation and Missile Command
Langley Research Center, Hampton, Virginia

National Aeronautics and
Space Administration

Langley Research Center
Hampton, Virginia 23681-2199

March 2000

Available from:

NASA Center for AeroSpace Information (CASI)
7121 Standard Drive
Hanover, MD 21076-1320
(301) 621-0390

National Technical Information Service (NTIS)
5285 Port Royal Road
Springfield, VA 22161-2171
(703) 605-6000

Summary

Development of advanced rotorcraft configurations has highlighted a need for high-quality experimental data to support the development of flexible and accurate analytical design tools. To provide this type of data, a test program was conducted in the NASA Langley 14- by 22-Foot Subsonic Tunnel to measure the flow near the empennage of a 15-percent scale powered helicopter model with an operating tail fan. Three-component velocity profiles were measured forward of the horizontal tail for four advance ratios using laser velocimetry (LV) to evaluate the effect of the rotor wake impingement on the horizontal tail angle of attack. These velocity data indicate the horizontal tail can experience unsteady angle of attack variations of over 30° due to the rotor wake influence. The horizontal tail is most affected by the rotor wake above advance ratios of 0.10. Velocity measurements of the flow on the inlet side of the tail fan were also made for a low-speed flight condition using LV techniques. The velocity data show an accelerated flow near the tail fan duct, and vorticity calculations track the passage of main rotor wake vortices through the measurement plane.

Introduction

As rotor and fuselage designs become more integrated, compact, and complex, rotor-wake-fuselage aerodynamic interactions are an increasingly important part of the overall performance characteristics of rotorcraft. Reference 1 attributes the importance of interactional effects for modern helicopters to increased disk loading, more compact designs, low-level flight requirements, and the increased requirement for directional trim after the loss of the tail rotor that results in larger vertical tail surfaces. These effects are especially important in the design and placement of the anti-torque system, such as a tail rotor, and the horizontal and vertical stabilizers as documented in references 2-3.

Much work has already been done experimentally and analytically to define the interaction effects between the rotor and the fuselage (refs. 4-15). A more limited amount of experimental data is available for analyzing the main rotor/anti-torque interactions (refs. 16-22). Advanced configurations such as the RAH-66 are designed and manufactured with sophisticated and new anti-torque devices, and there is a need for high-quality experimental data to support the development of more flexible analytical models capable of treating these types of configurations (refs. 23 and 24). Reference 25 specifically cites the difficulty in predicting unsteady empennage loads at speeds below 40 knots. Reference 26 provides experimental pressure data at model scale for a generic T-tail empennage, and reference 27 discusses the tremendous amount of testing involved in the Light Helicopter (LH) design process. However, there does not appear to be specific information in the literature on the velocities in the flowfield of a lifting rotor near an operating tail fan.

In order to investigate the rotor wake-fuselage-empennage interactions near the empennage of a powered small-scale helicopter with an operating tail fan and a T-tail, the U. S. Army Joint Research Program Office, Aeroflightdynamics Directorate, in cooperation with the NASA Langley Research Center,

conducted a wind tunnel test program in the 14- by 22-Foot Subsonic Tunnel. Velocity data were acquired forward of the horizontal tail for four flight conditions to document the unsteady downwash near the horizontal tail. Velocity data were also obtained on the inlet side of the tail fan for one flight condition, providing information about the inflow into the tail fan.

Symbols and Abbreviations

C_T Rotor thrust coefficient, $\frac{T}{\rho\pi R^2(\Omega R)^2}$

R Rotor radius, ft

T Rotor thrust, lb

u Streamwise component of velocity, ft/sec

U_∞ Freestream velocity, ft/sec

v_f Induced velocity in forward flight, ft/sec

v_h Induced velocity in hover, ft/sec

v Lateral component of velocity, ft/sec

w Vertical component of velocity, ft/sec

x, y, z Cartesian coordinates (see fig. 3), in.

α Rotor shaft angle, positive nose up, deg

μ Main rotor advance ratio, $\frac{U_\infty}{\Omega R}$

X Wake skew angle, deg, $\tan^{-1}\left[\frac{U_\infty\cos(\alpha)}{v_f - U_\infty\sin(\alpha)}\right]$

Ω Main rotor rotational speed, rad/sec

ρ Density of air, slugs/ft^3

BL Baseline reference configuration: fuselage, tail fan covered with plates

FDP Frequency Domain Processor

LV Laser Velocimetry

MR Main rotor configuration: fuselage, tail fan free-wheeling, main rotor operating

MRTF Main rotor/tail fan configuration: fuselage, tail fan operating, main rotor operating

OR Order Ratio, frequency spectrum of velocity signal in multiples of rotor fundamental frequency

TF Tail Fan configuration: fuselage, tail fan operating

2MRTS 2-Meter Rotor Test System

Model and Instrumentation

The test program was conducted in the Langley 14- by 22-Foot Subsonic Tunnel using the Army's 2-Meter Rotor Test System (2MRTS) with a four-bladed, 15-percent scale rotor, a fuselage model representative of the RAH-66, and the tunnel's three-component laser velocimetry (LV) system.

The 14- by 22-Foot Subsonic Tunnel is a closed-circuit, atmospheric wind tunnel designed for the low-speed testing of powered and high-lift configurations (ref. 28). In the open test section configuration, the walls and ceiling are lifted out of the flow, leaving a solid floor under the model. In this configuration, the tunnel can achieve a maximum dynamic pressure of about 92 lb/ft^2. This investigation was conducted with the tunnel in the open test section configuration to allow complete optical access to the rotor flowfield. For this test program, the test section

floor was lowered two feet to install the LV optics. A false floor with a window, flush with the rest of the tunnel, was placed over the LV optics.

Figure 1 shows the 2MRTS ready for testing in the tunnel. The LV system is also visible in the photograph. The rotor system, which was installed on the 2MRTS, had a 4-bladed, articulated hub with blades that closely matched the planform, twist, and airfoils of the RAH-66 blades. No attempt was made to dynamically scale these blades. Because the only hub available for testing was a 4-bladed hub, there were some deviations from scale from an actual model of the 5-bladed RAH-66. The radius of the blades when installed on the 4-bladed hub was reduced by one inch from a true 15-percent scale RAH-66. In addition, the use of only four blades reduced the rotor solidity and resulted in higher blade loads for any given thrust coefficient. The blades and hub are described in more detail in table 1 and a planform sketch of the blades is shown in figure 2. The 2MRTS is described in further detail in reference 29.

The fuselage was a 15-percent scale model of the RAH-66 and was instrumented with over 200 surface pressure ports and 4 dynamic pressure gages. Forces and moments on the rotor and fuselage were measured separately by two six-component, strain-gage balances. The fuselage is shown in detail in figure 3. Fuselage surface pressure data were acquired during this test program, and samples of the pressure data are used in reference 30 for computational fluid dynamics (CFD) code calibration.

The anti-torque device of the configuration was modeled by an air-powered, tip-driven, 8-in. diameter, 22-bladed fan mounted in the tail fan duct. The fan configuration is shown in figure 4. As can be seen in the photograph, the fan duct section was painted black to minimize the optical reflections from the surface. Although the fan configuration did not match the physical 8-bladed tail fan assembly of the full-scale configuration, the model fan was used to simulate the general flow physics and trim conditions for the model by using the fan rpm to control the fan thrust. For this study, a general simulation of the thrusting fan environment was thought to be sufficient to yield information regarding the flowfield around the fuselage. Obviously, a detailed assessment of the full-scale fan design could not be made using this type of simulation.

Laser Velocimeter System

The LV system was a three-component system operated in the backscatter mode to minimize alignment difficulties between the transmit and receive optics packages. Most components of the system are described in references 31-32; this paper presents the first data obtained with the upgraded three-component system. The streamwise and vertical components of velocity are measured by optics located on the side of the tunnel, out of the flow; the lateral crossflow component of velocity is measured by optics which are located beneath the tunnel floor. The traversing mechanisms of the three components are computer-controlled to ensure the sample volumes of the three sets of beams are positioned at a single location. As can be seen in figure 1, the third component beams originating beneath the floor were angled at 33° relative to the vertical. This angle was necessary to optically access the inflow area of the tail fan due to the cant of the tail fan duct. Corrections for this rotation in the lateral velocity component were applied to the data during post-processing.

Except for its long focal length and zoom lens assembly, the system was a standard fringe-based LV system. Polystyrene particles (1.7 micron) suspended in an alcohol and water mixture were used to seed the flow. The velocity data were acquired using frequency domain processors (FDP's) to maximize the signal to noise ratio of the data. The LV data acquisition system was designed to allow acquisition of rotor azimuth position in addition to the velocity measurements so that an

"azimuthal history" of the velocity could be reconstructed in post-processing.

Measurement Locations and Test Procedures

The laser velocimeter measurement locations are described briefly below and are shown in figure 5. The operating conditions for each configuration are documented in table 2.

Horizontal Tail

LV data were obtained for ten points in a vertical line one chord forward and one chord (mid-semi-span) to the right of center of the horizontal tail with both the main rotor and tail fan operating (MRTF) for main rotor advance ratios of 0.055, 0.076, 0.102, and 0.150. The rotor thrust coefficient was 0.007, and the rotor shaft angle was held at a constant -0.65°.

Tail Fan

In order to investigate non-linear interference effects between the main rotor wake and the tail fan, velocity data were acquired on the inlet side of the tail fan for several combinations of unpowered and powered main rotor and tail fan conditions.

Baseline Data were acquired for a baseline reference condition (BL), which consisted of only the fuselage (no main rotor installed) and the tail fan covered with plates to prevent flow through the tail duct. This established the reference flow conditions at the measurement plane due to just the presence of the fuselage in the freestream. The tunnel speed was 55 ft/sec, which was the speed for a main rotor advance ratio of 0.076 if the main rotor had been installed and operating. The velocity was measured with LV in three locations near the covered tail fan. At each location, the velocity was very close to the freestream value, indicating little interference due to the fuselage alone at these locations.

TF For the tail fan operating alone condition (TF), the main rotor was not installed, and the tail fan was operated at an rpm which was known to generate about 340 in-lbs of anti-torque. This was the amount of anti-torque that was predicted before the test program to be required to trim the configuration in yaw. The tunnel speed was again set to 55 ft/sec. Measurements of velocity with the LV were made at a limited number of locations as reflections from the tail fan spinner and the duct made the measurements difficult to acquire with the LV system operating in the backscatter mode.

MR LV measurements were obtained in the same measurement plane for the main rotor operating alone condition (MR). This configuration had the main rotor installed and operating, and the tail fan was uncovered and unpowered, but it did free-wheel during the test condition. The tail fan was uncovered to minimize the optical reflections from the cover. As a result, the tail fan was free-wheeling at a nominal rpm of about 150. This was approximately 3% of the operating rpm for the fan; however, during static thrust sweeps of the fan, it required 1200 rpm to generate 0.3 lbs of fan thrust. Therefore, the free-wheeling fan rpm of 150 was considered too low in magnitude to generate any significant thrust or create any measurable flow effects. In addition, the fuselage yawing moment did not vary greatly between this configuration and the BL configuration, so it was not expected that this change from covered fan to free-wheeling fan would appreciably affect the data comparisons.

The operating conditions were a main rotor advance ratio of 0.076, a thrust coefficient of 0.0051, and a shaft angle of -0.60°. The main rotor was trimmed to zero longitudinal and lateral first harmonic flapping. Due to the relatively small size of the model and the low thrust coefficient, the calculated wind tunnel wall effects corrections were insignificant, and no wall corrections were applied to these data. Measurements of the rotor torque averaged 330

in-lbs, indicating the TF anti-torque setting was very close to that required for trimming the system for the MR configuration. Measurements of velocity were made with LV at more locations near the tail fan for this configuration as it was assumed that the rotor wake would cause more non-uniform distribution of velocity than either the BL or the TF configuration.

MRTF The final configuration was for both the main rotor and tail fan operating (MRTF). In this configuration, the main rotor was trimmed in the same manner as for the MR configuration with the advance ratio = 0.076, the thrust coefficient = 0.0051, and the shaft angle = -0.63°. The tail fan was operated at the same rpm and pressure as for the TF configuration. However, although the fan rpm was approximately the same as for the TF configuration, the anti-torque produced was 640 in-pounds, almost twice as much as needed to trim the model to zero yawing moment. This increased performance by the tail fan may be due to the favorable interference effects between the rotor wake and the tail fan. This favorable interference resulted in a model test configuration that was out of trim in yaw when compared to a flight test condition. Unfortunately, there was not enough testing time to acquire a second MRTF test condition for better trim matching.

It was noted during the test program that for this operating condition, the model would occasionally shake or "twitch" in yaw; this observed phenomenon indicated the fan might have been experiencing some type of inlet stall phenomenon. The main concentration of LV measurements was for this MRTF configuration.

LV Data Acquisition and Reduction

The LV data acquisition process consisted of placing the sample volume at the measurement location and acquiring data for a period of nine minutes or until 4096 velocity measurements were made in each of the longitudinal, vertical, and lateral components of velocity. The LV measurements were not made in coincidence, which would have required that each component of velocity be measured at the same time from the same particle. Instead, the flow was assumed to be periodic with rotor blade passage, and each component was allowed to be measured individually; this dramatically reduced the time required to obtain the LV data. During this process, as was mentioned earlier, conditional sampling techniques were employed to associate each measured velocity with the azimuth of the rotor blades at the time when the measurement was made. At the conclusion of the process, the measurement location was changed, and the acquisition process was repeated.

For each measurement location, the raw data were reviewed, and the histograms of the velocities in each of the three components were processed to improve the signal-to-noise ratio. The data were "binned" into 128 bins (2.8° azimuth each), and the mean velocity for the location was calculated from the mean of all the azimuth bins. Since the data were associated with a rotor position, it was possible to sort the data by azimuthal position, thereby reconstructing a time history of velocity at each measurement location that represented one average rotor revolution.

The largest contributors to the uncertainty in the LV measurements are the measurement of the crossbeam angle and the particle lag. Using the error estimation techniques described in references 32-34, the LV system error for the velocity measurements in this paper is estimated at 1.3% measured velocity.

Discussion of Results

Horizontal Tail Velocity Measurements

The average downwash angle, as measured

using LV at a location one chord forward of the horizontal tail, is shown in figure 6 for several advance ratios. In each of these cases, both the main rotor and the tail fan are operating at the conditions indicated in table 2. As expected, the downwash angle decreases with increasing advance ratio. Similarly, the average sidewash angle is shown in figure 7. The sidewash angle decreases with increasing advance ratio; that is, the average lateral flow tends more to the starboard side of the model with increasing forward speed.

Large variations in the unsteady downwash and sidewash angles were also measured using the LV system. Typical plots of the unsteady flow angles calculated from the unsteady velocity data are shown in figure 8 for a height one-half inch below the horizontal tail for each of the advance ratios tested. The results indicate over 30° of unsteady fluctuation are encountered near the horizontal tail at the blade passage frequency with the most unsteadiness occurring at an advance ratio of 0.10. Carpet plots of the unsteady angles for all the advance ratios that were tested are presented in figure 9. These plots show the variation in unsteady angle with height above the tail section at each advance ratio.

From the unsteady data, an experimental determination of the position of the rotor wake relative to the horizontal tail can be made by analyzing the 4/rev content of the velocity. The vertical component of velocity was used to calculate the 4/rev RMS content of the rotor wake, and the results are shown in figure 10. The strong 4/rev content indicates that the rotor wake is the dominant flow feature. Figure 10 also shows the position of the rotor wake relative to the horizontal tail for the advance ratios tested. In figure 10, the tail is immersed in the wake above advance ratios of 0.10 as shown by the high 4/rev content at all measurement locations for these advance ratios. These results generally agree with those in reference 26, considering the different geometry and flight conditions of the two test configurations.

A theoretical evaluation of the wake skew angle can be made based on the equations in reference 35. Generally accepted practice in applying the equations of reference 35 to calculate wake skew angle is to use the hover induced velocity, v_h, in the equation for wake skew angle. Since v_h is defined as:

$$v_h = \sqrt{\frac{T}{2\rho\pi R^2}}$$

this is a fairly straightforward calculation. However, in determining the wake skew angle for a forward flight configuration, the induced velocity in forward flight, v_f, can be shown to be a function of thrust, tip speed, and forward speed. By solving the equation and assuming that the rotor shaft angle is small, v_f is given by:

$$v_f = \frac{1}{\sqrt{2}}\sqrt{\left(\sqrt{\left[C_T{}^2(\Omega R)^4 + U_\infty{}^4\right]} - U_\infty{}^2\right)}$$

The skew angle is then calculated by:

$$X = \tan^{-1}\left[\frac{U_\infty \cos(\alpha)}{v_f - U_\infty \sin(\alpha)}\right]$$

This formulation for X using the forward-flight induced velocity results in a significantly different skew angle calculation than if the hover value of induced velocity is used. The results of the skew angle calculation are plotted in figure 11 along with the geometry of the configuration. In figure 11, the calculated wake skew angle, which theoretically defines the edge of the rotor wake, is shown to approach the position of the horizontal tail at advance ratios of 0.10 and above. This correlates well with the experimental determination of rotor wake position shown in figure 10.

Figure 12 illustrates an interesting feature of the unsteady vertical flow near the horizontal tail. At the lower advance ratios of the test

program, represented by the sample plot in figure 12a, the flow is dominated by the 4/rev blade-passage frequency and its multiples. At an advance ratio of 0.15, a significant 2/rev content becomes present in the flow as shown in figure 12b. Reference 26 also reports a strong 8/rev in the flow near the horizontal tail; the data in the present investigation show periodic content at several multiples of the 4/rev frequency, as well as frequencies between the multiples of the 4/rev. During the inflow studies of references 36-38, 2/rev frequencies were noted in several instances; it is possible these frequencies are generated by vorticity shed from the hub and pylon that moves into the measurement area at the increased advance ratios.

Tail Fan Velocity Measurements

Figure 13 presents contour plots in the fan system coordinates of the average streamwise velocity, u, the lateral (perpendicular to the fan) velocity, v, and the vertical (parallel to the fan) velocity, w, on the inlet side of the duct. These are presented for the MRTF configuration operating at the conditions listed in table 2. Note the accelerated flow at the forward section of the duct. The photographs in figure 14 show surface flow visualization of the empennage for one of the runs. The flow visualization, supported by the velocity data, indicate the flow is separated along the upper half of the upstream lip of the tail fan duct. The photographs also show a large region of separation on the aft part of the tail fan shroud. There are also several separation lines on the vertical tail and the junction between the vertical tail and the tail fan duct. This occurs on both the right and left hand side of the empennage.

The purpose of acquiring data for several different model configurations was to allow the determination of the non-linear interference effects between the main rotor wake and the tail fan flow. This was determined by subtracting the combination of the MR and TF velocities from the MRTF velocities. The results for four locations in the measurement plane are given in table 3. There are limited results for this part of the investigation due to the small number of measurements made for the TF configuration. From a percentage standpoint, the non-linear effects are most significant in the lateral velocity (v) component, which is influenced the most by the tail fan flow.

For each measurement location, the unsteady, azimuthally-dependent velocity was measured by LV in each velocity component. For a given azimuth, the velocity at each measurement point can be extracted and plotted on a contour plot to give an effective velocity "snapshot" of the entire measurement grid. As these data were processed at azimuth intervals of 2.8°, there were 128 snapshots of velocity in each of the three components.

From each snapshot of velocity, the vorticity component normal to the measurement grid plane was calculated for the MRTF configuration. By examining each azimuthal "snapshot", it became evident that areas of concentrated vorticity were convecting through the measurement plane. Figure 15 shows examples of two azimuth angles. Both positive (into the plane) and negative vorticity are present in the plots. The phenomenon occurs 4 times per revolution as would be expected due to the 4-bladed rotor configuration. This periodic content in the data indicates that the main rotor blade wake vortices are passing through the measurement plane at the blade passage frequency. The rotor wake contains both positive and negative vorticity due to the geometric structure of the blade tip vortices. Whether the vortices are seen as positive or negative is dependent on the wake age and the vortex origination point. Wake flow visualization of this phenomenon can be found in reference 39.

The convection velocities, on average, were calculated to be 45 ft/sec in the downstream direction and 52 ft/sec in the vertical direction. This equates to an experimental skew angle of

41°. Using the equations in the above section for skew angle, the calculated momentum skew angle is determined to be 62°. Although the calculation and the data have a 21° difference in skew angle, this can be explained by the difference in the inflow velocity data between momentum theory and experimental measurement. It is known from references 36-40 that the experimental inflow for this type of rotor contains more downwash on the aft portion of the disk than is predicted by momentum theory. Therefore, it is expected that the experimental skew angle would be less in magnitude than the skew angle calculated from momentum theory.

Conclusions

In order to investigate the rotor wake-fuselage-empennage interactions near the empennage of a powered small-scale helicopter with an operating tail fan and a T-tail, the U. S. Army Joint Research Program Office, Aeroflightdynamics Directorate, in cooperation with the NASA Langley Research Center, conducted a wind tunnel test program in the 14- by 22-Foot Subsonic Tunnel. Velocity data were acquired forward of the horizontal tail for four flight conditions, documenting the unsteady downwash near the horizontal tail. Velocity data were also obtained on the inlet side of the tail fan for one flight condition, providing information about the inflow into the tail fan. The major conclusions from this study are:

1. The horizontal tail surface experiences large changes (over 30°) in the unsteady sidewash and downwash angles due to the influence of the rotor wake. The horizontal tail is most affected by the rotor wake above advance ratios of 0.10.

2. The wake skew angle, calculated through solving the momentum equation for induced velocity, can be significantly different than the experimental value.

3. There is an accelerated flow pattern near the operating tail fan. Flow visualization, as well as the measured velocity data, indicate the flow is separated on part of the forward duct lip and at the base of the vertical tail for an advance ratio of 0.07 and a main rotor thrust coefficient of 0.005.

4. Velocity measurements show the passage of vorticity at the inlet to the tail fan. Both positive and negative vorticity are measured in the flowfield, and the vorticity is convected at an angle and rate consistent with passage of the rotor wake through the tail fan inlet area.

References

1. Sheridan, P. F.; and Smith, R. P.: Interactional Aerodynamics--A New Challenge to Helicopter Technology. *Proceedings of the 35th Annual Forum*, American Helicopter Soc., 1979.

2. Roesch P.; and Vuillet, A.: New Designs for Improved Aerodynamic Stability on Recent Aerospatiale Helicopters. *Proceedings of the 37th Annual Forum*, American Helicopter Soc., 1981.

3. Prouty, R. W.; and, Amer, K. B.: The YAH-64 Empennage and Tail Rotor--A Technical History. *Proceedings of the 38th Annual Forum*, American Helicopter Soc., 1982.

4. Ahmed, S. R.; Raddatz, J.; and Hoffman, W.: Analysis of Helicopter Rotor-Fuselage Interference with Time Averaged Pressure Distribution. *Proceedings of the 17th European Rotorcraft Forum*, Berlin, 1991.

5. Ahmed, S. R.; and Meyer, F. W.: A Mach-Scaled Powered Model For Rotor-Fuselage Interactional Aerodynamics And Flight Mechanics Investigations. *Proceedings of the International Specialists' Meeting on Rotorcraft Basic Research*, American Helicopter Soc., 1991.

6. Bettschart, N.; Hanotel, R.; Ilbas, D.; and Desopper, A.: *Theoretical And Experimental Studies Of Helicopter Rotor/Fuselage Interaction.* ONERA TP 1991-198, 1991.

7. Norman, T. R.; and Yamauchi, G. K.: Full-Scale Investigation Of Aerodynamic Interactions Between A Rotor And Fuselage. *Proceedings of the 47th Annual Forum*, American Helicopter Soc., 1991.

8. Berry, J. D.: *RWF Rotor-Wake-Fuselage Code Software Reference Guide.* NASA TM 104078, 1991.

9. Leishman J. G.; and Bi, N. P.: Measurements Of A Rotor Flowfield And The Effects On A Fuselage In Forward Flight. *Proceedings of the 16th European Rotorcraft Forum*, Glasgow, 1990.

10. Lorber, P. F.; and Egolf, T. A.: An Unsteady Helicopter Rotor-Fuselage Aerodynamic Interaction Analysis. *Journal of the American Helicopter Society*, Vol. 35, (3), 1990.

11. Meyer, F. W.: The Influence Of Interactional Aerodynamics Of Rotor-Fuselage-Interference On The Fuselage Flow. *Vertica*, Vol. 14, (2), 1990.

12. Dehondt, A.; and Toulmay, F.: Influence Of Fuselage On Rotor Inflow Performance And Trim. *Vertica*, Vol. 14, (4), 1990.

13. Wilson, F. T.: *Fuselage Aerodynamic Design Issues And Rotor/Fuselage Interactional Aerodynamics. Part 1: Practical Design Issues.* AGARD, Aerodynamics of Rotorcraft, N91-18048, 1991.

14. Rand, O.; and Gessow, A.: Model For Investigation Of Helicopter Fuselage Influence On Rotor Flowfields. *Journal of Aircraft*, Vol. 26, May 1989.

15. Trept, T.: *A 0.15-Scale Study Of Configuration Effects On The Aerodynamic Interaction Between Main Rotor And Fuselage.* NASA CR-166577, 1984.

16. Huber, H.; and Polz, G.: *Studies on Blade-to-Blade and Rotor-Fuselage-Tail Interferences.* In AGARD Prediction of Aerodynamic Loads on Rotorcraft, N83-17470-08-01, 1983.

17. Fitzgerald, J.; and Kohlhepp, F.: *Research Investigation Of Helicopter Main Rotor/Tail Rotor Interaction Noise.* NASA CR-4143, 1988.

18. Jacobs, E. W.; Fitzgerald, J. M.; and Shenoy, R. K.: Acoustic Characteristics Of Tail Rotors And The Effects Of Empennage Interactions. *Proceedings of the 43rd Annual Forum*, American Helicopter Soc., 1987.

19. Balch, D. T.: *Experimental Study Of Main Rotor Tip Geometry And Tail Rotor Interactions In Hover.* NASA CR 177336, 1985.

20. Balch, D. T.; Saccullo, A.; and Sheehy, T. W.: *Experimental Study Of Main Rotor/Tail Rotor/Airframe Interactions In Hover.* NASA CR-166485, 1983.

21. Edwards, B. D.; Peryea, M. A.; and Brieger, J. T.: 0.15 Scale Model Studies Of Main And Tail Rotor Interaction. *Proceedings of the National Specialists' Meeting on Aerodynamics and Aeroacoustics*, American Helicopter Soc., 1987.

22. Martin, R. M.; Burley, C. L.; and Elliott, J. W.: *Acoustic Test Of A Model Rotor And Tail Rotor: Results For The Isolated Rotor And Combined Configuration.* NASA TM 101550, 1989.

23. Pagnano, G.; and Saporiti, A.: Current European Research Activities In Helicopter Interactional Aerodynamics. *Proceedings of the 17th European Rotorcraft Forum*, Berlin, 1991.

24. Philippe, J.: ONERA Makes Progress In Rotor Aerodynamics, Aeroelasticity, and Acoustics. *Vertiflite*, Sept/Oct. 1992, pp. 48-53.

25. Torok, M. S.; and Ream, D. T.: Investigation of Empennage Airloads Induced by a Helicopter Main Rotor Wake. *Proceedings of the 49th Annual Forum*, American Helicopter Soc., 1993.

26. Moedersheim, E.; and Leishman, J. G.: Investigation of Aerodynamic Interactions Between a Rotor and a T-Tail Empennage. *Proceedings of the Aeromechanics Specialist Meeting*, American Helicopter Soc., 1995.

27. Keys, C.; Sheffler, M.; Weiner, S.; and Heminway, R.: LH Wind Tunnel Testing: Key

to Advanced Aerodynamic Design. *Proceedings of the 47th Annual Forum*, American Helicopter Soc., 1991.

28. Gentry, G. L.; Quinto, P. F.; Gatlin, G. M.; and Applin, Z. T.: *The Langley 14- by 22-Foot Subsonic Tunnel: Description, Flow Characteristics, And Guide For Users.* NASA TP 3008, 1990.

29. Phelps, A. E.; and, Berry, J. D.: *Description of the Army's 2-Meter Rotor Test System.* NASA TM-87762, AVSCOM TM-86-B-4, 1987.

30. Duque, E. P. N.; Berry, J. D.; Budge, A. M.; and Dimanlig, A. C. B.: A Comparison of Computed and Experimental Flowfields of the RAH-66 Helicopter. *Proceedings of the Aeromechanics Specialist Meeting, American Helicopter Soc.*, 1995.

31. Mace, W. D. Jr.; Elliott, J. W.; Blancha, B.; and Murphy, J.: Comparison Of Frequency Domain And Time Domain Laser Velocimeter Signal Processors. *14th International Congress on Instrumentation in Aerospace Simulation Facilities*, 1991.

32. Gorton, S. A.; Poling, D. R.; and Dadone, L.: *Investigation Of Blade-Vortex Interaction Using Laser Velocimetry And Pressure-Instrumented Rotor Blades. Volume 1—Advance Ratio of 0.2, Rotor Lift Coefficient Normalized by Solidity of 0.07, and Shaft Angle of 0 Degrees.* NASA TM 4570, ATCOM-TR-94-A-003, 1995.

33. Young, W. H., Jr.; Meyers, J. F.; and Hepner, T. E.: *Laser Velocimeter Systems Analysis Applied to a Flow Survey Above a Stalled Wing.* NASA TN D-8408, 1977.

34. Dring, R. P.: Sizing Criteria for Laser Anemometry Particles. *J. Fluids Eng.*, vol 104, Mar. 1982, pp. 15-17.

35. Stepniewski, W. Z.; and Keys, C. N.: *Rotary-Wing Aerodynamics.* Dover Publications, Inc., New York, 1984, p. 64.

36. Elliott, J. W.; Althoff, S. L.; and Sailey, R. H.: *Inflow Measurements Made with a Laser Velocimeter on a Helicopter Model in Forward Flight— Volume I: Rectangular Planform at an Advance Ratio of 0.15.* NASA TM 100541, AVSCOM TM 88-B-004, 1988.

37. Elliott, J. W.; Althoff, S. L.; and Sailey, R. H.: *Inflow Measurements Made with a Laser Velocimeter on a Helicopter Model in Forward Flight—Volume II: Rectangular Planform at an Advance Ratio of 0.23.* NASA TM 100542, AVSCOM TM 88-B-005, 1988.

38. Elliott, J. W.; Althoff, S. L.; and Sailey, R. H.: *Inflow Measurements Made with a Laser Velocimeter on a Helicopter Model in Forward Flight—Volume III: Rectangular Planform at an Advance Ratio of 0.30.* NASA TM 100543, AVSCOM TM 88-B-006, 1988.

39. Ghee, T. A.; Berry, J. D.; and Zori, L. A. J.: *Wake Geometry Measurements and Analytical Calculations on a Small-Scale Rotor Model.* NASA TP-3584, 1996.

40. Hoad, D. R.: *Rotor Induced-Inflow-Ratio Measurements and CAMRAD Calculations.* NASA TP-2946, AVSCOM-TM-89-B-010, 1990.

Tables

Table 1. Description of rotor blades.

Airfoil sections	
23.7-percent radius	VR-12
84.6-percent radius	VR-12
91.8-percent radius	SSC-A09
100-percent radius	SSC-A09
Chord, in.	
23.7-percent radius	2.25
74.3-percent radius	2.25
91.8-percent radius	2.25
100-percent radius	1.35
Cutout, in.	8.2
Flapping hinge offset, in.	2.0
Lag hinge offset, in.	2.0
Number of blades	4
Pitch axis, percent of chord	25
Radius, in.	34.55
Solidity, thrust-weighted	0.07866
Tip sweep angle (of 1/4 chord), deg	30
Tip sweep begins, in.	31.7
Twist, deg	
0-percent radius	0
23.7-percent radius	0
74.3-percent radius	-6.6
84.6-percent radius	-7.6
91.8-percent radius	-9.5
100-percent radius	-9.5

Table 2. Test Conditions.

Variable	BL	TF	MR	MRTF	Horizontal Tail			
Advance ratio	—	—	0.076	0.076	0.055	0.076	0.102	0.15
Collective, deg	—	—	7.1	7.4	11.0	10.1	8.9	7.5
Density, slug/ft^3	.00249	.00243	.00242	.00241	.00236	.00237	.00236	.00235
Fuselage angle of attack, deg	4.3	4.4	4.3	4.3	4.1	4.0	4.1	4.1
Freestream velocity, ft/sec	54.9	55.0	55.2	55.2	40.0	54.7	73.8	108.9
Freestream velocity, knots	32.6	32.6	32.7	32.7	23.7	32.4	43.7	64.5
Fuselage yaw moment, in-lb	-25.7	-342.8	-75.0	-641.9	-473.4	-631.3	-815.5	-781.4
Lateral cyclic, deg	—	—	1.1	1.1	1.2	1.3	1.9	2.5
Longitudinal cyclic, deg	—	—	-3.0	-3.0	-2.8	-3.0	-3.2	-2.7
Rotor drag, lb	—	—	2.1	1.7	0.6	2.8	2.6	3.3
Rotor lift, lbs	—	—	170.0	169.0	230.5	228.9	229.4	228.8
Rotor rpm	—	—	2401	2400	2400	2399	2402	2401
Rotor shaft angle, deg	—	—	-0.60	-0.63	-0.66	-0.61	-0.61	-0.61
Rotor thrust coefficient	—	—	.00512	.00512	.00714	.00706	.00707	.00709
Rotor yawing moment, in-lb	—	—	330.3	324.4	540.3	497.2	421.8	310.0
Tail fan rpm	—	5007	—	5394	4860	5197	6262	5435

Table 3. Non-linear Interference Velocities.

Location (measured from center of fan)	MRTF - (MR + TF), ft/sec			Velocity, % MRTF, ft/sec		
	u	*v*	*w*	*u*	*v*	*w*
1 inch upstream, 0.7 inch up	-3.5	2.9	-9.1	-4.0	-18.8	11.6
1 inch downstream, 0.7 inch up	-6.7	0.9	-7.8	-8.3	-4.6	10.0
1 inch upstream, 2.7 inch up	-3.9	6.9	-6.2	-4.7	-34.8	7.5
1 inch downstream, 2.7 inch up	-6.9	5.2	-15.9	-9.3	-23.3	19.9

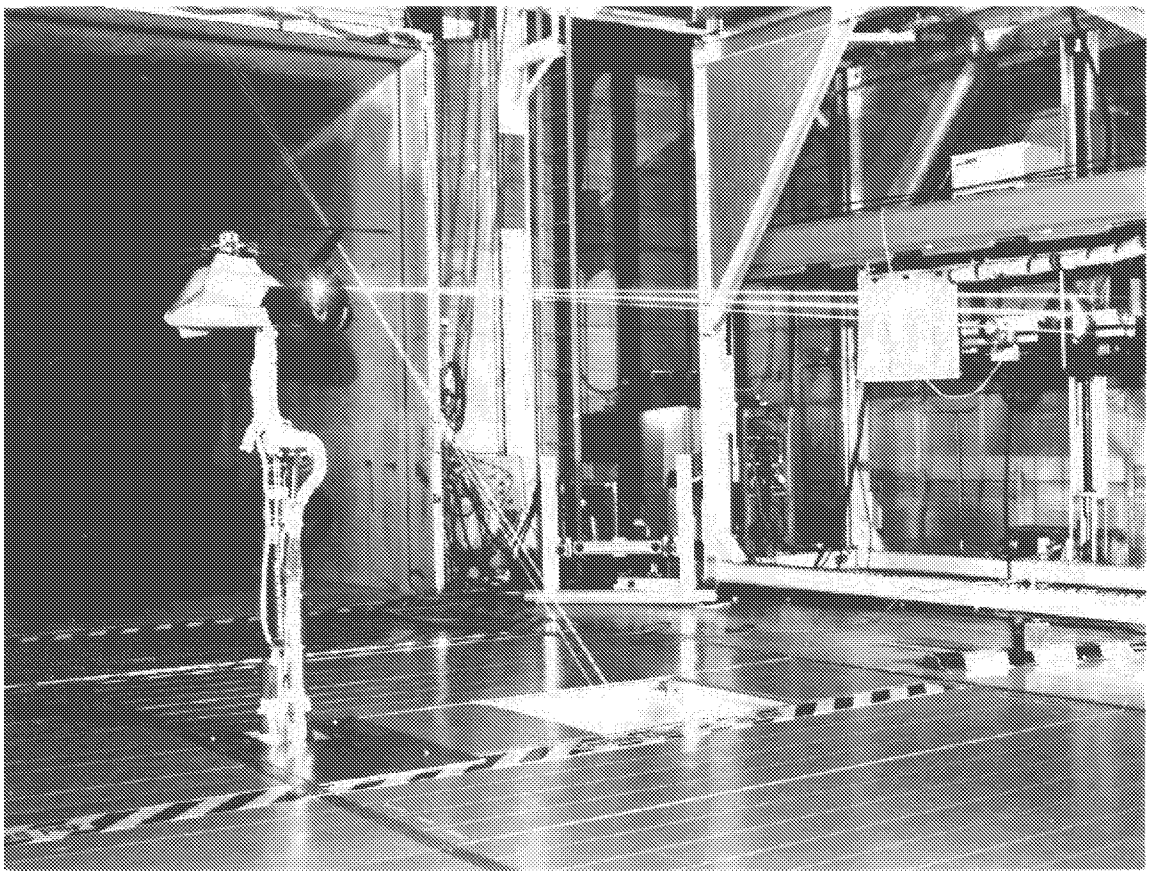

L-95-1069

Figure 1. Model and LV system installed in tunnel.

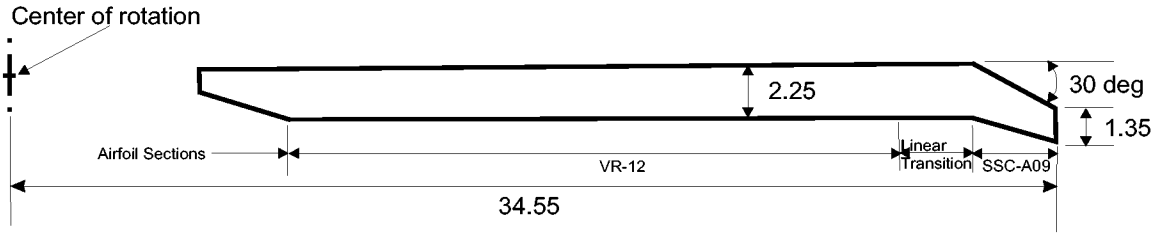

Figure 2. Description of blade planform. All dimensions in inches.

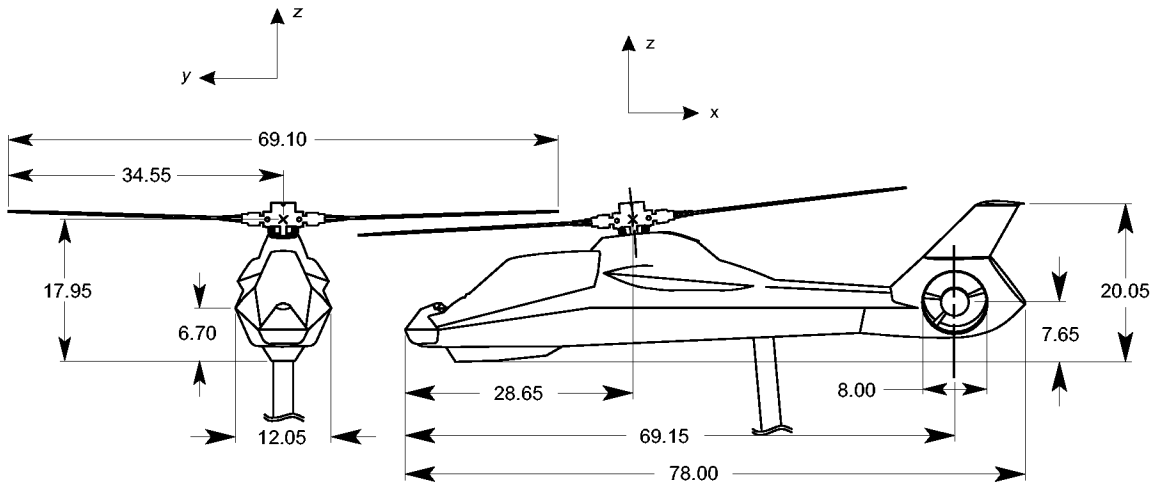

Figure 3. Description of fuselage. All dimensions in inches.

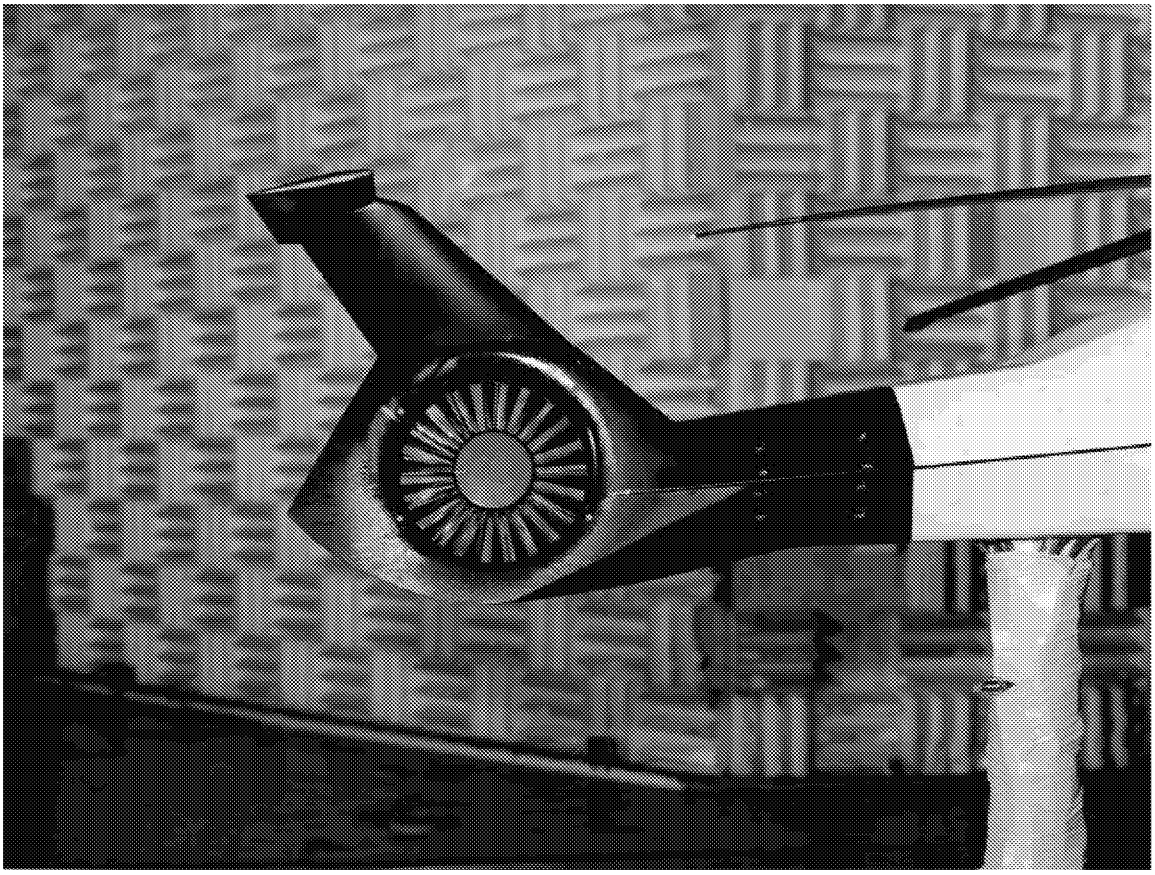

L-95-1071

Figure 4. Tail fan configuration.

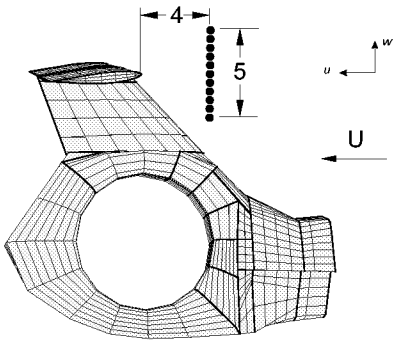

(a) Side view of horizontal tail measurement locations.

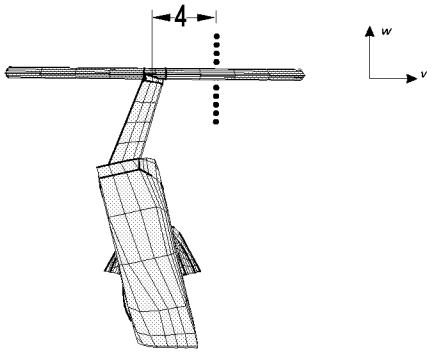

(b) Rear view of horizontal tail measurement locations.

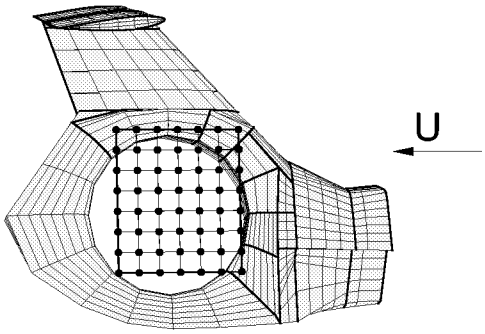

(c) Side view of fan measurement locations.

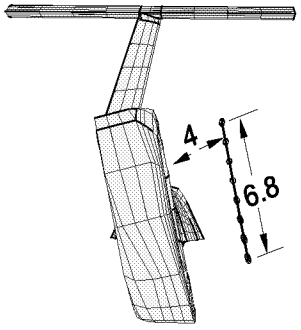

(d) Rear view of fan measurement locations.

Figure 5. Velocity measurement locations. All dimensions in inches.

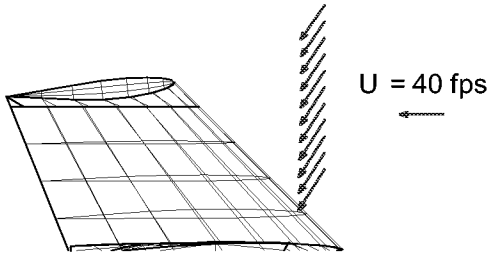

(a) $\mu = 0.05$. Average downwash angle is 57 degrees.

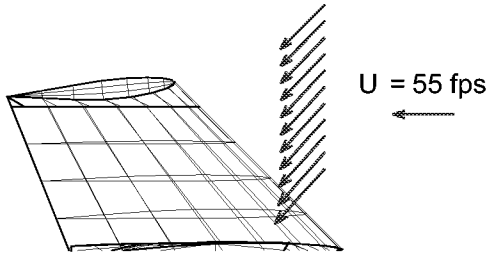

(b) $\mu = 0.07$. Average downwash angle is 47 degrees.

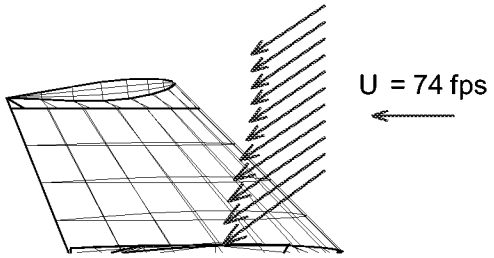

(c) $\mu = 0.10$. Average downwash angle is 35 degrees.

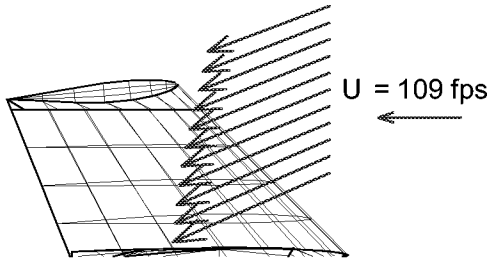

(d) $\mu = 0.15$. Average downwash angle is 23 degrees.

Figure 6. Average downwash angle forward of the horizontal tail for MRTF.

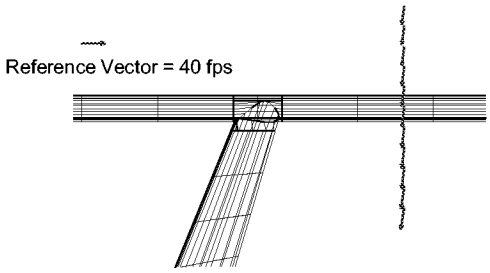

(a) $\mu = 0.05$. Average sidewash angle is 11 degrees.

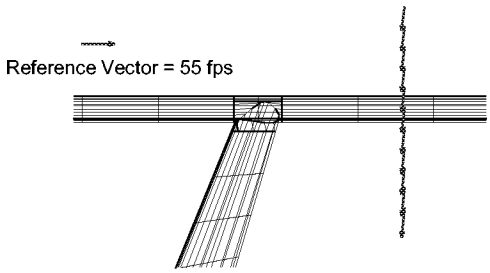

(b) $\mu = 0.07$. Average sidewash angle is 7 degrees.

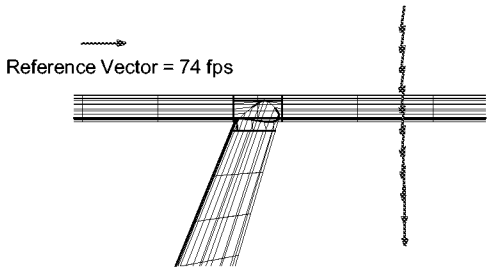

(c) $\mu = 0.10$. Average sidewash angle is 4 degrees.

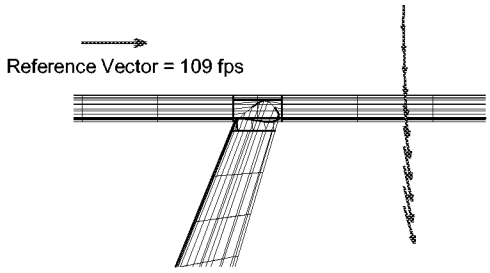

(d) $\mu = 0.15$. Average sidewash angle is -3 degrees.

Figure 7. Average sidewash angle forward of the horizontal tail for MRTF.

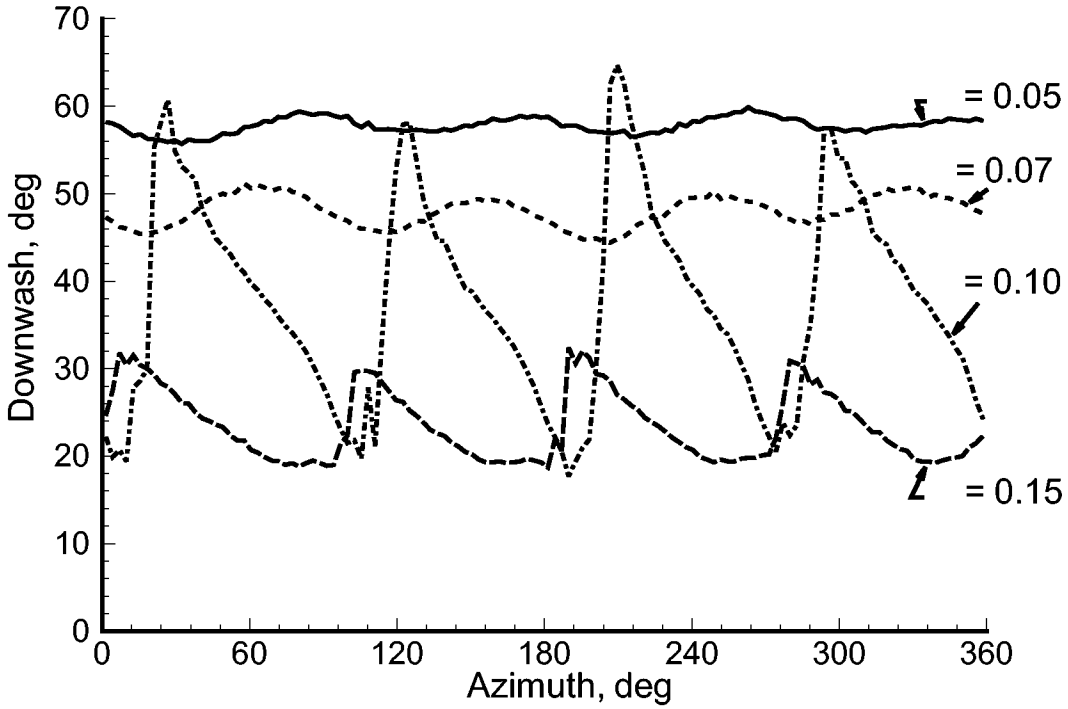

(a) Downwash angle.

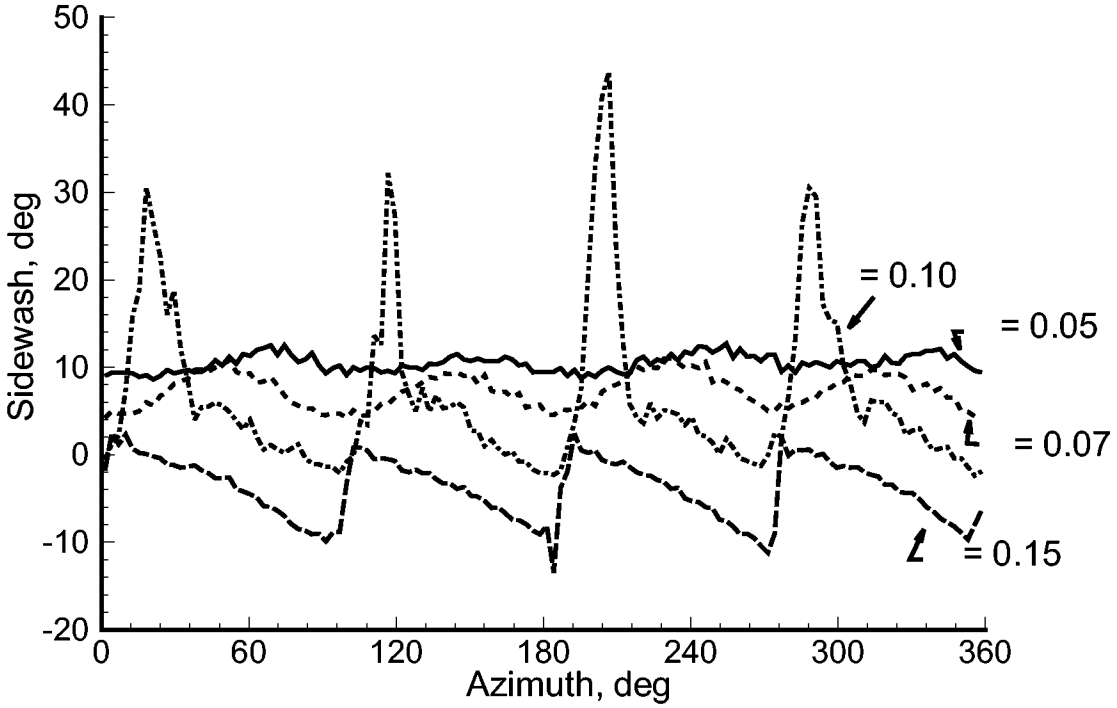

(b) Sidewash angle.

Figure 8. Unsteady angles for a location 0.5 inches below the horizontal tail.

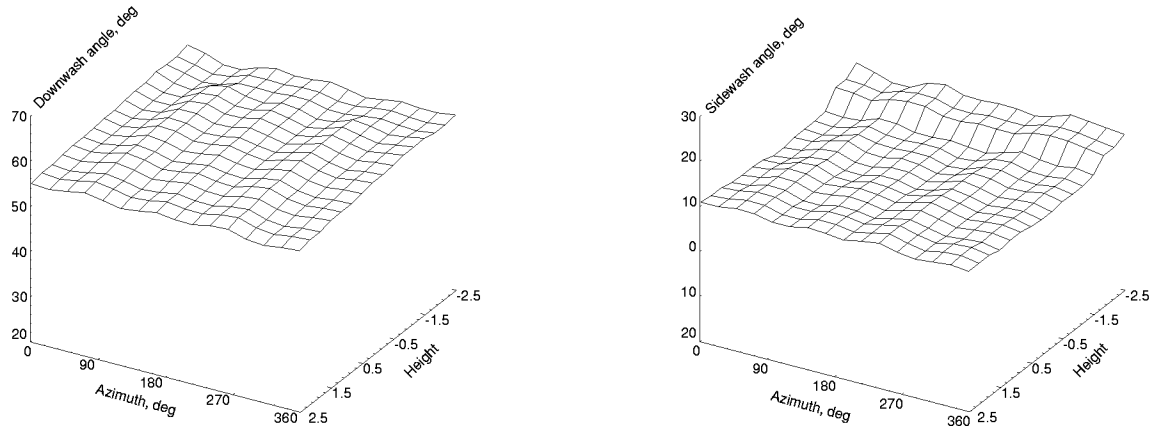

(a) $\mu = 0.05$.

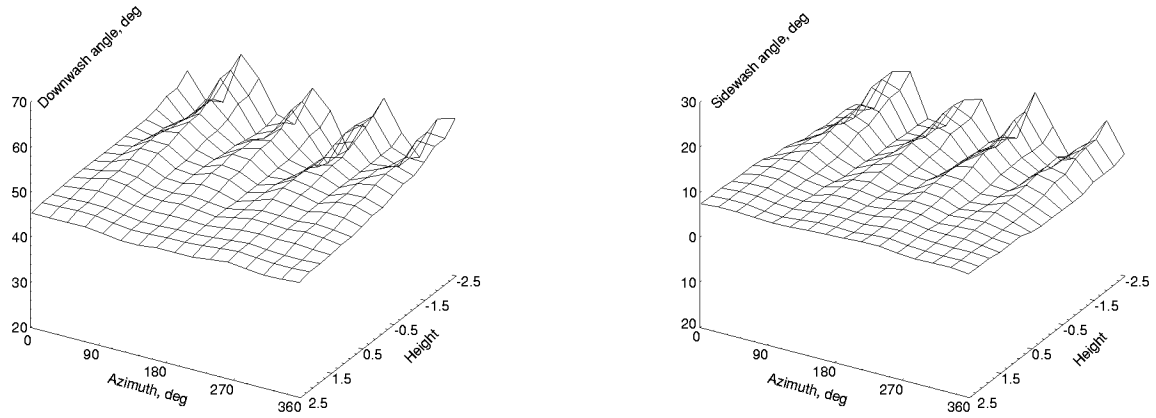

(b) $\mu = 0.07$.

Figure 9. Unsteady downwash and sidewash angles for MRTF.

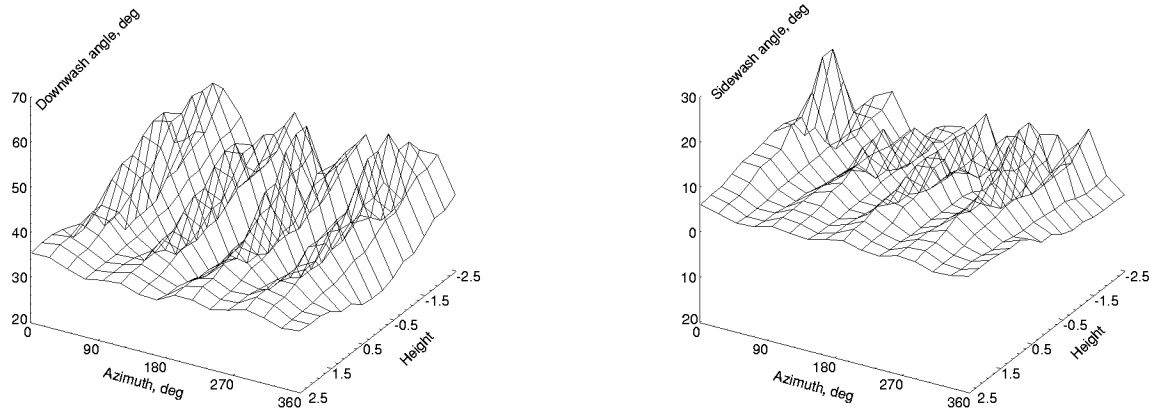

(c) $\mu = 0.10$.

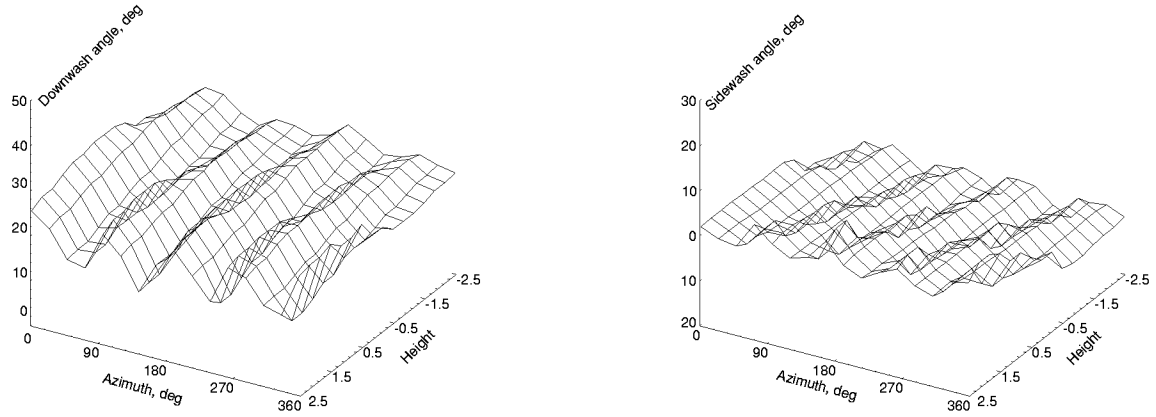

(d) $\mu = 0.15$.

Figure 9. Concluded.

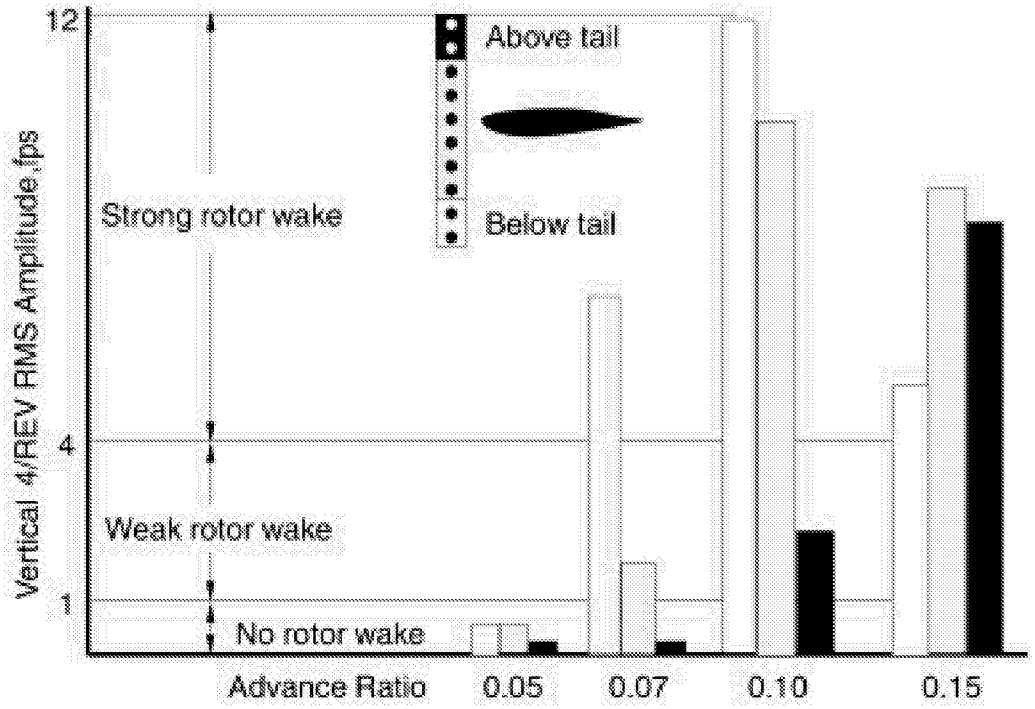

Figure 10. Unsteady vertical wake impingement at horizontal tail for MRTF.

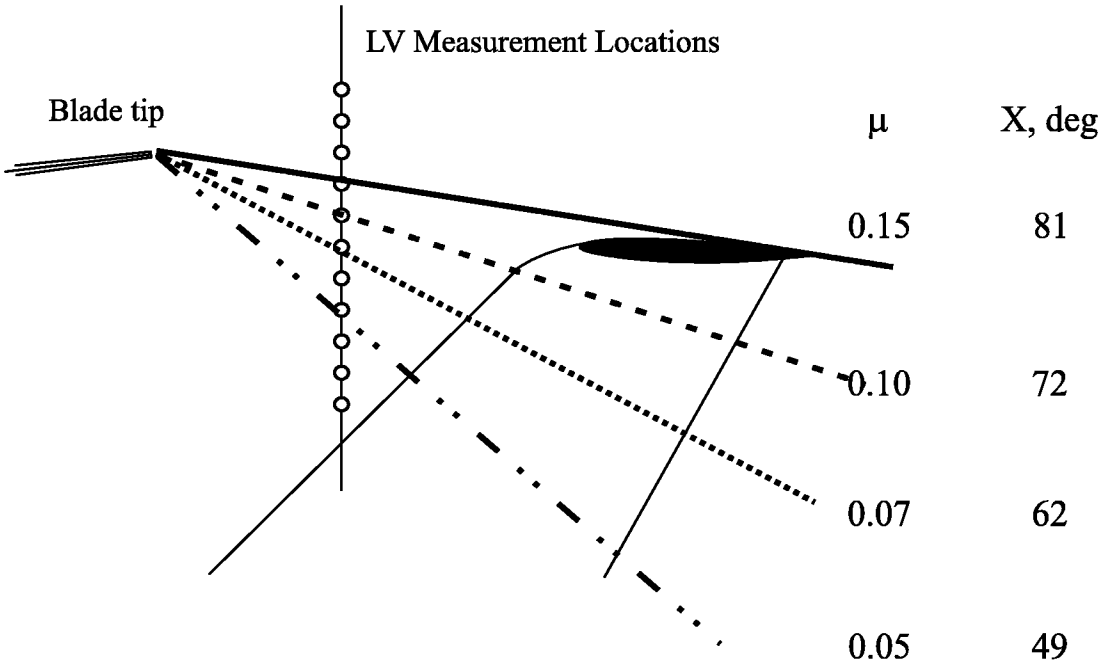

Figure 11. Wake skew angle calculation for $C_T = 0.007$ projected on model geometry.

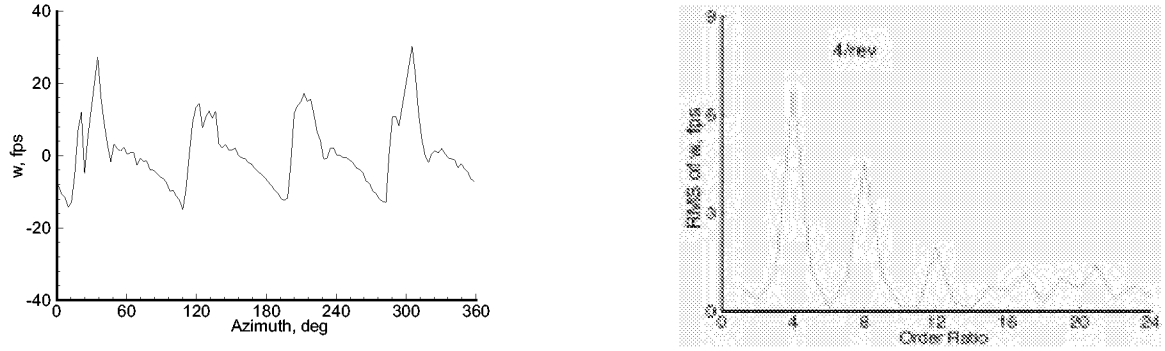

(a) $\mu = 0.10$.

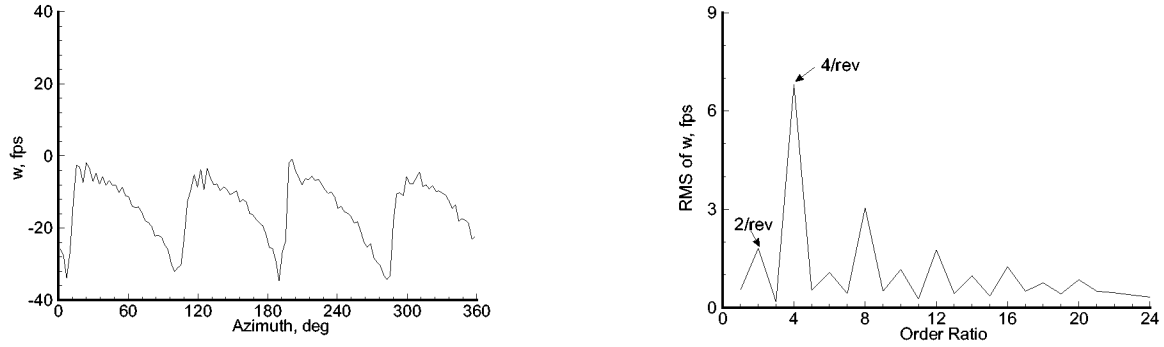

(b) $\mu = 0.15$.

Figure 12. Velocity and order ratio analysis for location 2 inches below centerline of horizontal tail, MRTF.

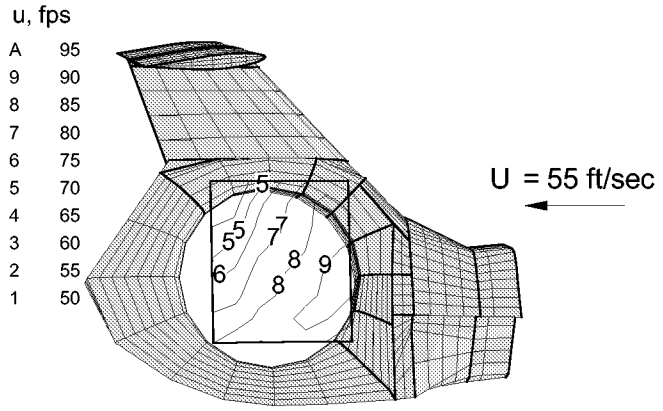

(a) Streamwise velocity, *u*.

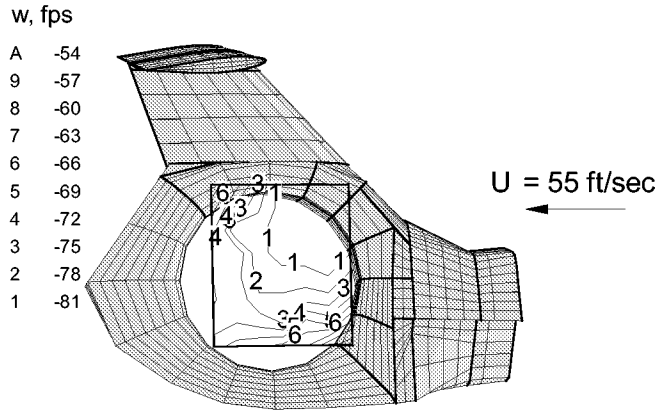

(b) Vertical velocity, *w*.

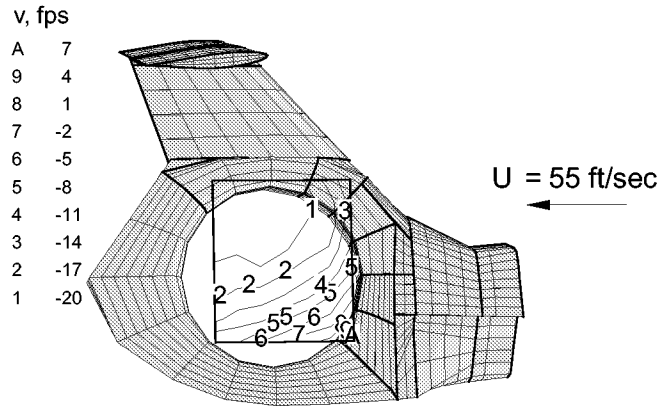

(c) Lateral velocity (inflow), *v*.

Figure 13. Contour plots of LV average velocity data for MRTF configuration.

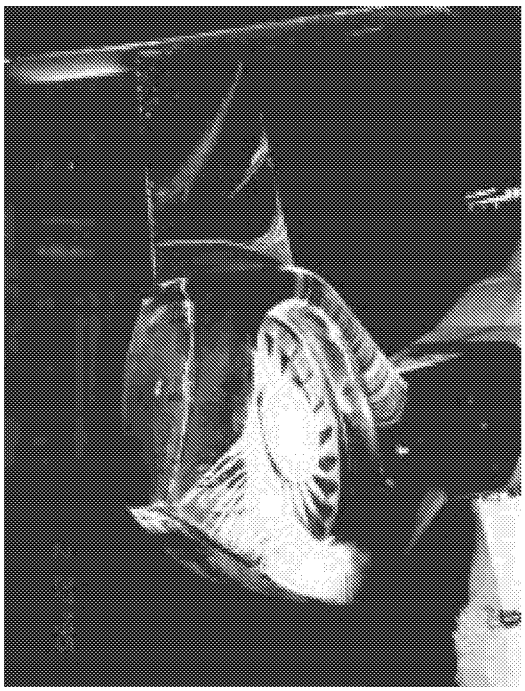

(a) Inlet side of tail fan.

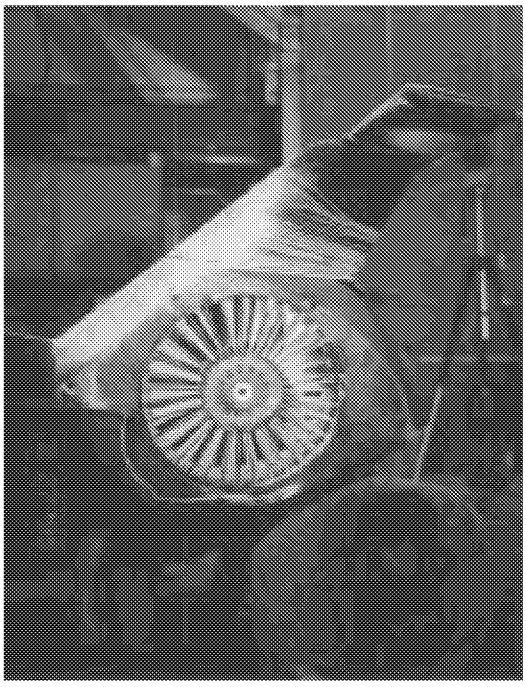

(b) Outflow side of tail fan.

Figure 14. Surface flow visualization of empennage for μ = 0.07 and thrust coefficient of 0.005, MRTF configuration.

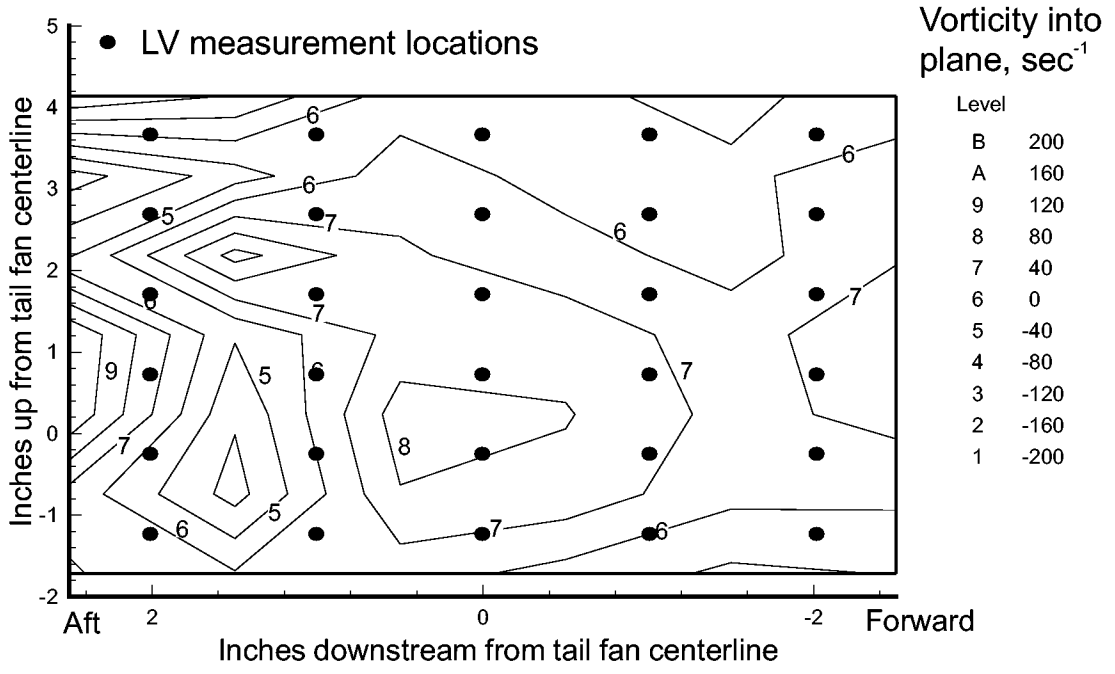

(a) Azimuth = 150 degrees.

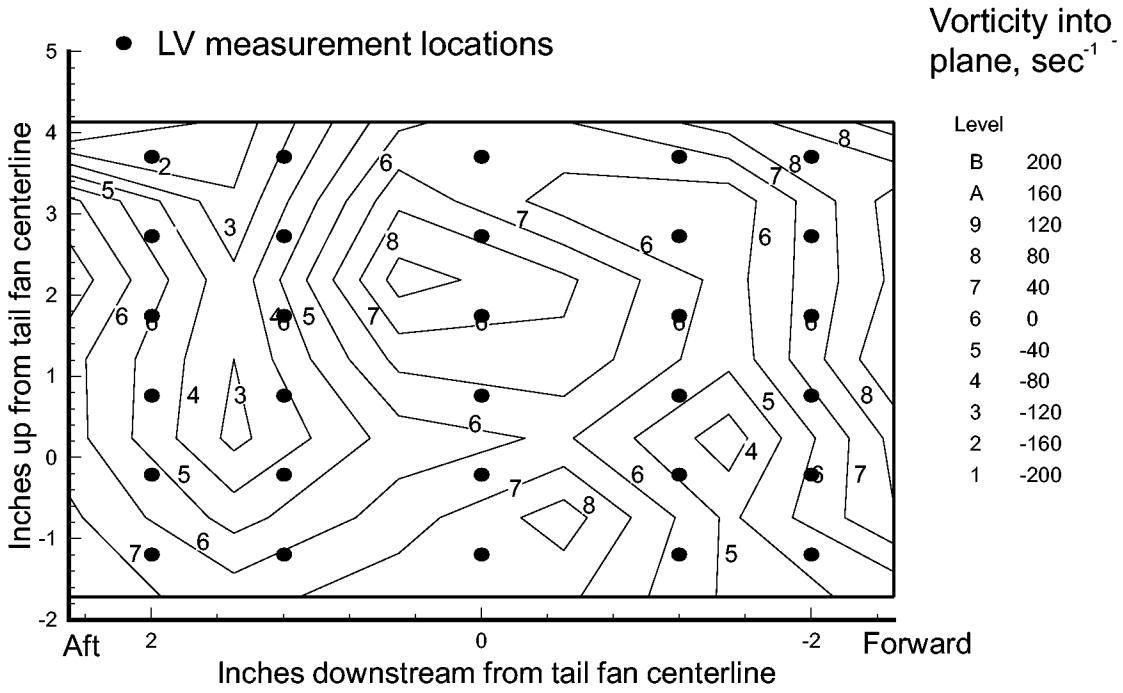

(b) Azimuth = 220 degrees.

Figure 15. Vorticity contours calculated from unsteady LV data for MRTF configuration.

REPORT DOCUMENTATION PAGE

Form Approved
OMB No. 0704-0188

1. AGENCY USE ONLY (*Leave blank*)	2. REPORT DATE	3. REPORT TYPE AND DATES COVERED
	March 2000	Technical Publication

4. TITLE AND SUBTITLE
Flow Environment Study Near the Empennage of a 15-Percent Scale Helicopter Model

5. FUNDING NUMBERS
WU 581-10-11-01

6. AUTHOR(S)
Susan Althoff Gorton, John D. Berry, W. Todd Hodges, Deane G. Reis

7. PERFORMING ORGANIZATION NAME(S) AND ADDRESS(ES)
NASA Langley Research Center
Hampton, VA 23681-2199

U.S. Army Aviation and Missile Command
Aeroflightdynamics Directorate
Joint Research Programs Office
NASA Langley Research Center
Hampton, VA 23681-2199

8. PERFORMING ORGANIZATION REPORT NUMBER
L-17940

9. SPONSORING/MONITORING AGENCY NAME(S) AND ADDRESS(ES)
National Aeronautics and Space Administration
Washington, DC 20546-0001
and
U.S. Army Aviation and Missile Command
Moffett Field, CA 94035-1000

10. SPONSORING/MONITORING AGENCY REPORT NUMBER
NASA/TP-2000-210085
AFDD/TR-00-A-004

11. SUPPLEMENTARY NOTES
Berry: U.S. Army Aviation and Missile Command, Directorate of Aviation Engineering, Redstone Arsenal, Huntsville, AL 35898

12a. DISTRIBUTION/AVAILABILITY STATEMENT
Unclassified-Unlimited
Subject Category 03 Distribution: Standard
Availability: NASA CASI (301) 621-0390

12b. DISTRIBUTION CODE

13. ABSTRACT (*Maximum 200 words*)
Development of advanced rotorcraft configurations has highlighted a need for high-quality experimental data to support the development of flexible and accurate analytical design tools. To provide this type of data, a test program was conducted in the Langley 14- by 22-Foot Subsonic Tunnel to measure the flow near the empennage of a 15-percent scale powered helicopter model with an operating tail fan. Three-component velocity profiles were measured with laser velocimetry (LV) one chord forward of the horizontal tail for four advance ratios to evaluate the effect of the rotor wake impingement on the horizontal tail angle of attack. These velocity data indicate the horizontal tail can experience unsteady angle of attack variations of over 30 degrees due to the rotor wake influence. The horizontal tail is most affected by the rotor wake above advance ratios of 0.10. Velocity measurements of the flow on the inlet side of the tail fan were made for a low-speed flight condition using conventional LV techniques. The velocity data show an accelerated flow near the tail fan duct, and vorticity calculations track the passage of main rotor wake vortices through the measurement plane.

14. SUBJECT TERMS
helicopter, rotor, wake, laser velocimetry, empennage, tail fan, fenestron, horizontal tail

15. NUMBER OF PAGES
30

16. PRICE CODE
A03

17. SECURITY CLASSIFICATION OF REPORT	18. SECURITY CLASSIFICATION OF THIS PAGE	19. SECURITY CLASSIFICATION OF ABSTRACT	20. LIMITATION OF ABSTRACT
Unclassified	Unclassified	Unclassified	UL